

## ECCENTRICITIES OF DOUBLE NEUTRON STAR BINARIES

CATHERINE MIA IHM<sup>1</sup>, VASSILIKI KALOGERA<sup>1</sup>, KRZYSZTOF BELCZYNSKI<sup>2</sup>*Submitted to The Astrophysical Journal, August 29, 2005*

## ABSTRACT

Recent pulsar surveys have increased the number of observed double neutron stars (DNS) in our galaxy enough so that observable trends in their properties are starting to emerge. In particular, it has been noted that the majority of DNS have eccentricities less than 0.3, surprisingly low values for systems that must stay bound after two supernovae. To investigate this trend, we generate many different theoretical distributions of DNS eccentricities using Monte Carlo population synthesis methods. We determine which eccentricity distributions are most consistent with the observed sample of DNS binaries. In agreement with Chaurasia & Bailes (2005), we find that highly eccentric, close DNS are less likely to be observed because of their accelerated orbital evolution due to gravitational wave emission and possible early mergers. Based on our results for close DNS, we also find that models with vanishingly or moderately small kicks ( $\sigma \lesssim 50 \text{ km s}^{-1}$ ) are inconsistent with the current observed sample of such DNS. We discuss the implications of our conclusions for DNS merger rate estimates of interest to ground-based gravitational-wave interferometers. We find that, although orbital evolution due to gravitational radiation affects the eccentricity distribution of the observed sample, the associated upwards correction factor to merger rate estimates is rather small (typically 10-40%).

*Subject headings:* binaries: general — binaries: close — stars: neutron — pulsars: general — gravitational waves

## 1. INTRODUCTION

Since the discovery of the Hulse & Taylor binary pulsar in 1974 (Hulse & Taylor 1975), seven more double neutron stars (DNS) have been found. Of these, five systems are considered “close” (or “coalescing”): PSRs B1913+16, B1534+12 (Wolszczan 1991), B2127+11C (Phinney & Sigurdsson 1991), J1756-2251 (Faulkner et al. 2004), and J0737-3039A (Burgay et al. 2003). Three are “wide” (or “noncoalescing”): PSRs J1518+4904 (Nice et al. 1996), J1811-1736 (Lyne et al. 2000), J1829+2456 (Champion et al. 2004). Binaries are characterized as either close or wide depending on their evolutionary timescales. A DNS goes through an inspiral phase and eventually merges because energy is taken away from its orbit in the form of gravitational radiation. If the time between the birth of the primordial binary and the merger of the resulting DNS is less than a Hubble time, we consider it to be “coalescing” (close), and “noncoalescing” (wide) if not. Coalescing DNS are of interest to LIGO and other ground-based interferometers because DNS mergers are primary targets for gravitational-wave detectors. The relativistic nature of such inspiraling DNS make them objects of extreme interest for astrophysics and relativity studies.

Of the five coalescing DNS, PSR B2127-11C is a system with an eccentricity of 0.68, located in the globular cluster M15 (Phinney & Sigurdsson 1991). This system most likely did not form through the isolated evolution of a primordial binary, but instead has been influenced by cluster dynamics. Our calculations in the present paper

TABLE 1  
OBSERVED DNS<sup>a</sup> BINARIES

PSR	e	a ( $R_{\odot}$ )	$P_{orb}$ (days)
B1913+16	0.617	1.009	0.323
B1534+12	0.274	1.606	0.421
J1756-2251	0.181	1.187	0.320
J0737-3039	0.088	0.610	0.102
J1518+4904	0.249	8.634	8.634
J1811-1736	0.828	14.982	18.779
J1829+2456	0.139	3.117	1.176

<sup>a</sup>Eccentricity, projected semimajor axis, and orbital period of observed DNS. Information obtained from the Australia Telescope National Facility (ATNF) Pulsar Catalogue.

do not account for DNS formation in clusters, and therefore we will not include PSR B2127-11C in our analysis.

The orbital properties of the DNS binaries we consider here are given in Table 1. It is evident that five of the seven observed DNS have orbital eccentricities below 0.3. The noticeable trend towards low eccentricity DNS is puzzling; one would think that a binary surviving two supernovae, believed to impart velocity kicks of up to  $1000 \text{ km s}^{-1}$  (e.g., Hobbs et al. 2005, and references therein), would be typically highly eccentric. A class of low eccentricity DNS, which receive low velocity kicks at the birth of the second neutron star, has been proposed by van den Heuvel (2004), as a possible explanation for the low eccentricities. However, evidence of large supernova kicks exists when looking at pulsar velocities (Hobbs et al. 2005; Arzoumanian et al. 2001; Lyne & Lorimer 1994).

In this paper we examine theoretical distributions of DNS eccentricities based on various model assumptions. These distributions are generated by Monte Carlo methods using binary evolution synthesis models (§ 2). We

<sup>1</sup> Northwestern University, Dept of Physics & Astronomy, Evanston, IL  
mia@alumni.northwestern.edu, vicky@northwestern.edu

<sup>2</sup> Tombaugh Fellow, Department of Astronomy, New Mexico State University, Las Cruces, NM 88003  
kbelczyn@nmsu.edu

analyze the resulting eccentricity distributions from a number of different models (§ 3), paying special attention to small vs. standard kicks and birth vs. present populations. We perform Bayesian statistical tests to evaluate whether any and which models are more likely, given the observed DNS sample (§ 4). In § 5, we show that high-eccentricity DNS are associated with shorter merger times and therefore they are harder to detect because of their early mergers, as also concluded by Chaurasia & Bailes (2005)<sup>3</sup>. We conclude with a discussion of our findings and their implications for DNS inspiral detections by ground-based gravitational-wave interferometers.

## 2. THEORETICAL METHODS

### 2.1. *StarTrack: Monte Carlo Population Synthesis*

To understand the observed sample of DNS and their eccentricities, we must provide a context for these observations by understanding the Galactic DNS population and their properties. Theoretical models of the stellar population are generated by population synthesis methods. Our population synthesis utilizes Monte Carlo techniques that randomly choose stellar parameters drawn from assumed distribution functions of initial conditions. These initial parameters characterize a primordial binary, and from these initial conditions the evolution of the binary is followed, based on best current our understanding of astrophysical processes. This is done for a large number of binaries, enough so that an adequate number of objects of interest form (in this case, DNS) for us to examine statistically.

We use the well-tested StarTrack Population Synthesis Code to generate a large number of binaries that simulates the population and evolution of binaries in our galaxy. A more complete description of the code can be found in Belczynski et al. (2001) and in Belczynski et al. (2005). Monte Carlo techniques are used to draw the initial parameters of the primordial binaries (masses, orbital separation, and eccentricity) from specified distributions, which are described in the next section. Furthermore the following are chosen from flat distributions: (a) the time of birth for each primordial binary, chosen from 0-15 Gyr, with a constant star formation rate assumed, (b) the direction and magnitude of the kick imparted to a neutron star (NS) or black hole (BH) in an asymmetric supernova (SN) explosion, and (c) the position in the orbit where the SN takes place (relevant to eccentric orbits before the explosion). Other aspects of the binary's evolution are based on physical laws that depend on the binary's properties with some necessary parametrizations.

We track the evolution of each binary and its physical properties at appropriate time steps from the zero-age main sequence until the formation of compact objects (white dwarfs, neutron stars, and black holes) and their subsequent orbital evolution. Effects such as stellar winds, stable and unstable mass transfer through Roche-lobe overflow and winds, angular momentum losses, supernovae, and orbital decay due to the emission of gravitational radiation are taken into account. The evolution

<sup>3</sup> We note that Chaurasia & Bailes (2005) appeared on the LANL preprint server when we were already preparing this manuscript for submission to the Journal.

of a binary ends when the binary merges, or when the end time of the simulation is reached (in this case, at 15 Gyr).

### 2.2. *Model Assumptions*

For this paper, we look at ten different population synthesis models, denoted as A, C, E1, G1, G3, H2, L1, L2, M1, and M2 [the name convention originates in Belczynski et al. (2001)]. Model A is our reference or *standard* model described next. All the other models are derived from this, with one of the synthesis model parameters varied.

The standard model draws masses for the primordial primary (the more massive binary component) from the initial mass function  $\Psi(M) \propto M^{-2.7}$  in the mass range from  $4M_{\odot}$  to  $100M_{\odot}$ , the masses relevant for neutron star and black hole formation. The binary mass ratio  $q$  defined as the ratio of the smaller mass to the larger, so  $0 < q \leq 1$ , is drawn from a flat distribution,  $\Phi(q) = 1$ , so that given a primary mass  $M_1$ , the mass of the secondary,  $M_2$ , is  $M_2 = qM_1$ . The initial separation of a binary is chosen from a distribution that is assumed to be logarithmically flat:  $\Gamma(A) \propto \frac{1}{A}$ . Initial eccentricities follow the thermal-equilibrium eccentricity distribution,  $\Xi(e) = 2e$ . For cases of dynamically unstable mass transfer and common-envelope evolution, we adopt an effective efficiency of  $\alpha_{CE} \times \lambda = 1$ ; neutron stars entering a common envelope phase are modeled taking into account hypercritical accretion. Helium star evolution is modeled in accordance to the results by Ivanova et al. (2003). Mass transfer phases between non-degenerate stars are assumed to be non-conservative (50% of the transferred mass is lost from the binary). This lost mass is assumed to carry a specific angular momentum equal to  $2\pi j A^2/P$  (i.e.,  $j = 1$ ). For supernova kicks imparted to neutron stars at birth we adopt the *joint* Maxwellian velocity distribution derived by Arzoumanian et al. (2001) with characteristic velocities  $\sigma_1 = 90$  km/s (weighted at 40%) and  $\sigma_2 = 500$  km/s (weighted at 60%). Hereafter we refer to this distribution of kicks as the “Arzoumanian kicks”.

The distinguishing characteristics of the other 9 models are described in Table 2. With this set of models we vary the values (within reasonable ranges) of a number of stellar and binary evolution parameters, that are known to affect DNS formation significantly. For more information on the specific choices of values for both the standard and these models, see Belczynski et al. (2001).

As a possible explanation of the low eccentricities, it has been suggested that a class of neutron stars forming in DNS systems that received small-magnitudes kicks is responsible for the observed low eccentricities (see van den Heuvel 2004, see also Pfahl et al. 2002). To investigate this suggestion statistically we created another 3 sets of models, in each of which different NS kick distributions are adopted (other than the Arzoumanian kicks): (i) a set of (unphysical in our opinion) models with zero NS kicks (all SN events are assumed to be symmetric); (ii) a set with a single Maxwellian of  $\sigma = 10 \text{ km s}^{-1}$ ; and (iii) a set with a single Maxwellian of  $\sigma = 50 \text{ km s}^{-1}$ . With these choices we hope to examine the effect of zero or low kick magnitudes on DNS orbital eccentricities. Each of these three kick distributions are adopted for all ten models listed in Table 2.

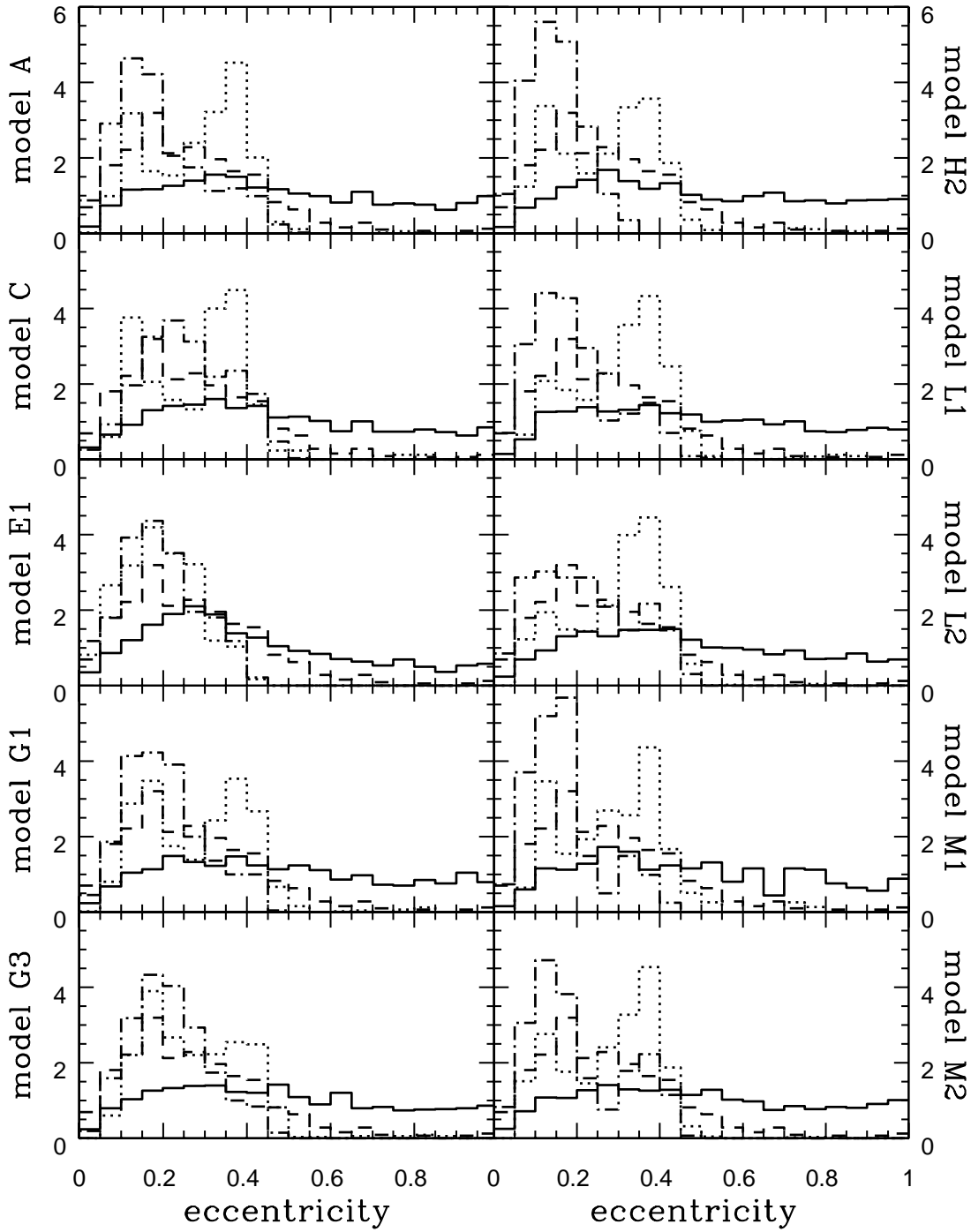


FIG. 1.— Eccentricity distribution functions for coalescing binaries at birth for the ten models in Table 1 and for four different NS kick assumptions: Arzoumanian kicks (solid lines), Maxwellian with  $\sigma = 50 \text{ km s}^{-1}$  (dashed lines), Maxwellian with  $\sigma = 10 \text{ km s}^{-1}$  (dash-dotted lines), and zero kicks (dotted lines). Only close binaries are considered.

### 3. PROBABILITY DISTRIBUTIONS

From the large populations of binaries we evolve, we consider all of the DNS systems formed and focus on the resultant DNS eccentricity distribution functions, for

each model. We typically generate  $\sim 30$  DNS for every  $10^5$  primordial binaries evolved, though in some cases  $10^5$  primordials will only produce a few relevant objects. In short, generating reliable statistics for a variety of different models is computationally expensive and requires

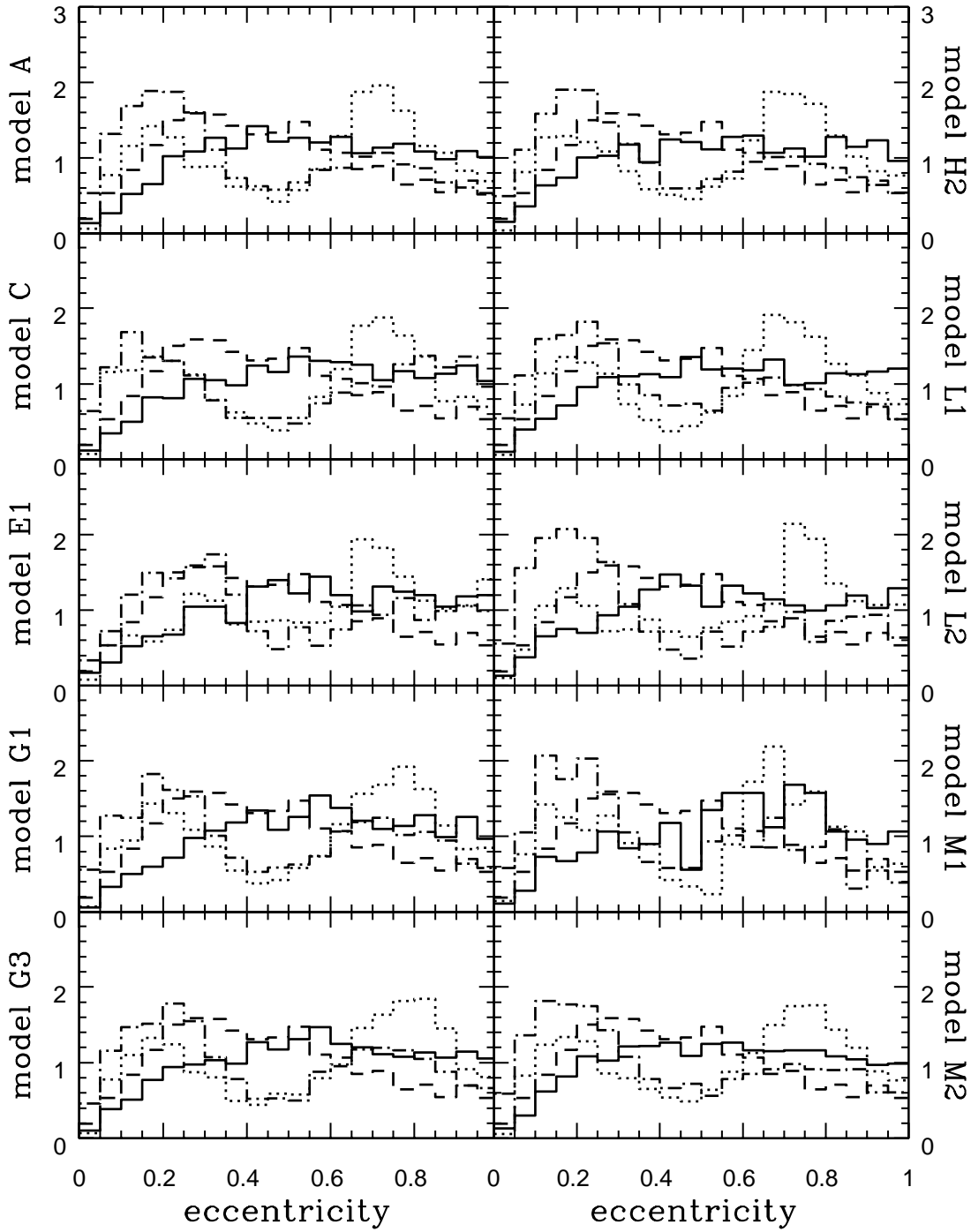


FIG. 2.— Eccentricity distribution functions for noncoalescing binaries at birth. Line types as in Fig. 1.

much time and patience. We make sure that for each model considered here we typically have model samples of  $2,000 - 3,000$  DNS at birth and at least  $\sim 200$  DNS for models that have atypically low DNS formation rates (e.g., L2, M1).

### 3.1. Zero, Low, and “Standard” Neutron-Star Kicks: Eccentricity Distributions at Birth

In Figs. 1 and 2 we present the eccentricity distribution functions at DNS birth, for all models considered in our study, and for coalescing and noncoalescing DNS,

TABLE 2  
MODEL ASSUMPTIONS

Model	Description
A	Standard (see text for details)
C	No hypercritical accretion onto NS/BH in common envelopes
E1	Effective common-envelope efficiency $\alpha_{CE} \times \lambda = 0.1$
G1,G3	Stellar winds reduced by $f_{wind} = 0.5, 0.2$
H2	Helium giants do not develop deep convective envelopes
L1,L2	Angular momentum of material lost in non-conservative mass transfer: $j = 0.5, 2.0$
M1,M2	Initial mass ratio distribution: $\Phi(q) \propto q^{-2.7}, q^3$

respectively. Before we proceed with our statistical analysis and comparison to the observed sample, there are a number of qualitative conclusions we can draw from these distributions.

In the case of coalescing DNS (Fig. 1), we find that the eccentricity distributions are distinctly different for the models with Arzoumanian (“standard”) kicks and those with zero or low kicks. In the first case the distribution covers the full range of values up to unity, and for most models it is almost flat-like across the range. As kick magnitudes decrease the distributions appear to be restricted to a low range of values, most typically below  $e = 0.5$ . This behavior appears to be consistent across all ten binary evolution models, independent of the specific model assumptions. This *qualitative* behavior is consistent with the suggestion made by van den Heuvel (2004) that very small NS kicks could be responsible for the low eccentricities in the observed sample.

For noncoalescing DNS (Fig. 2), the behavior of the eccentricity distributions is qualitatively different. For all kick choices, eccentricities cover the full range up to unity with no apparent qualitative difference or bias towards low values. For the (unphysical) case of zero NS kicks a double-peak structure is evident in most binary evolution models.

Further investigation of this structure reveals that it is due to a double-peak structure in the iron core masses of helium stars, the NS progenitors (as first revealed and discussed in detail by Timmes, Woosley, & Weaver (1996)). This structure propagates to the eccentricity through the mass-loss during the second supernova explosion in the systems: the range of helium-star masses is narrow, and therefore the double-peak structure persists in the distribution of mass amounts lost in the explosions; since the eccentricities for symmetric explosions is directly proportional to this SN mass loss, the double-peak signature is imprinted on the eccentricity distribution too. Once kicks are introduced (even of small magnitude) this structure is “washed-out” due to the randomizing effect of kicks. It turns out that this behavior has no effect on our statistical analysis that follows and therefore we do not discuss this in any further detail.

### 3.2. Birth vs. Present Distributions

We next compare the DNS eccentricity distributions (using models with Arzoumanian kicks) at two different times in their evolutionary history: at *birth* (the time when the second NS is formed) and at *present* (Fig. 3, 4), i.e., at 10 Gyr since the formation of the first primordial binaries in the simulations. Emission of gravitational radiation and resultant orbital inspiral, circularization, and mergers for the most short-lived DNS change the binaries’ orbital eccentricities as time progresses. We consider the present distributions a more realistic representation of the Galactic DNS population, since binaries must have experienced this kind of orbital evolution after their birth. In our simulations, each primordial binary is assigned (randomly) a formation time, and is subsequently tracked at regular time intervals so that it is possible to know the binary properties binary at a particular time.

It is evident that, for coalescing binaries (Fig. 3), there is a noticeable qualitative change of the present distributions towards lower eccentricities. This is in agreement with suggestions made and results obtained by Chaurasia & Bailes (2005). On the other hand, for non-coalescing DNS (Fig. 4) and for most binary evolution models, there is no clear evidence for significant evolution of the eccentricity distribution with time. We assert that this difference is due to the fact that the ages, i.e., time elapsed from their birth to the present, of most DNS binaries are short compared to the typical timescale relevant to orbital evolution due to gravitational radiation. Clearly this is consistent with the fact that these systems have such properties that do not coalesce within a Hubble time.

## 4. STATISTICAL ANALYSIS

In what follows we present the implementation of a Bayesian statistical analysis, following Finn (1994). This method allows us to compare the model predictions with the small-number observed samples, and calculate the likelihood of each of the models we consider here.

### 4.1. Method

#### 4.1.1. Observed Eccentricities

A priori it is not clear that the measured DNS eccentricities are indeed the true values, since measurements are associated with errors (no matter how small). Therefore, we assume that the measured eccentricities are distributed normally (following a Gaussian distribution) about the true value of each binary’s eccentricity:

$$P(e|\hat{e}, I) = \frac{\exp\left[-\frac{1}{2}\left(\frac{e-\hat{e}}{\sigma_e}\right)^2\right]}{\sqrt{2\pi}\sigma_e}. \quad (1)$$

Here,  $e$  corresponds to the observed eccentricity,  $\hat{e}$  is the true eccentricity, and  $\sigma_e$  is the reported uncertainty in the measurement.  $I$  is a parameter that encompasses all the unspecified assumptions that are also inherent in the observations. Note that we do not really know  $\hat{e}$ , the true value; we only know  $e$  and  $\sigma_e$ , which are the observations and errors of the seven DNS in the observed Galactic sample (Table 1). Of course, given the small errors associated with these measurements, the probability that the true value is very much different than the

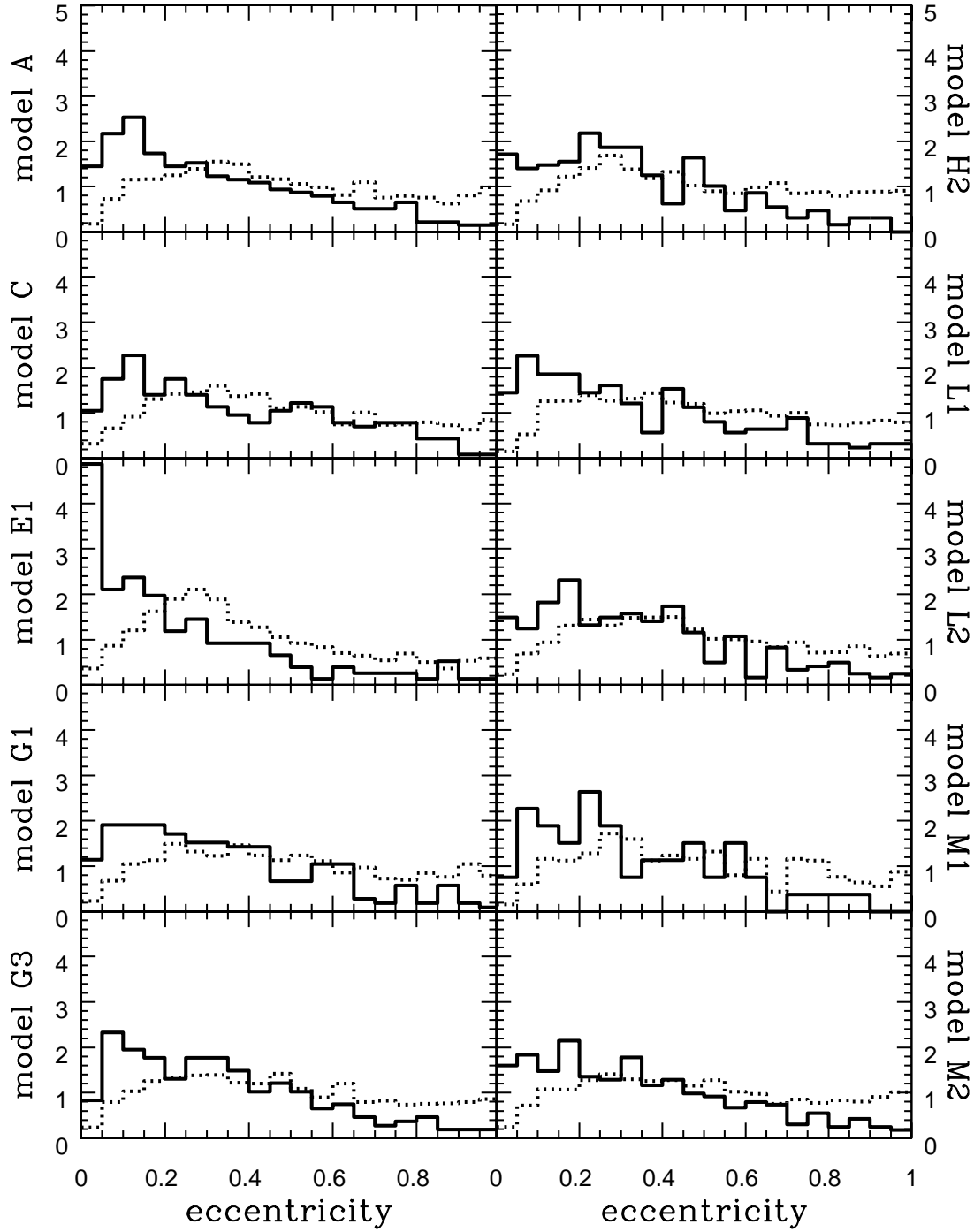


FIG. 3.— Eccentricity distribution functions for coalescing binaries for the ten models in Table 1 using Arzoumanian kicks. DNS populations are shown at birth (dotted lines) and at present (10 Gyr).

measured value is very small (lies in the tail of the Gaussian distribution).  $P(e|\hat{e}, I)$  will be used to describe the probability of individual eccentricities in our Bayesian analysis, which is described in the next section.

#### 4.1.2. Bayesian Statistics

In what follows we describe how we can use the observed sample and a set of theoretical eccentricity distributions to calculate the conditional probability that the observed sample is drawn from a particular theoretical

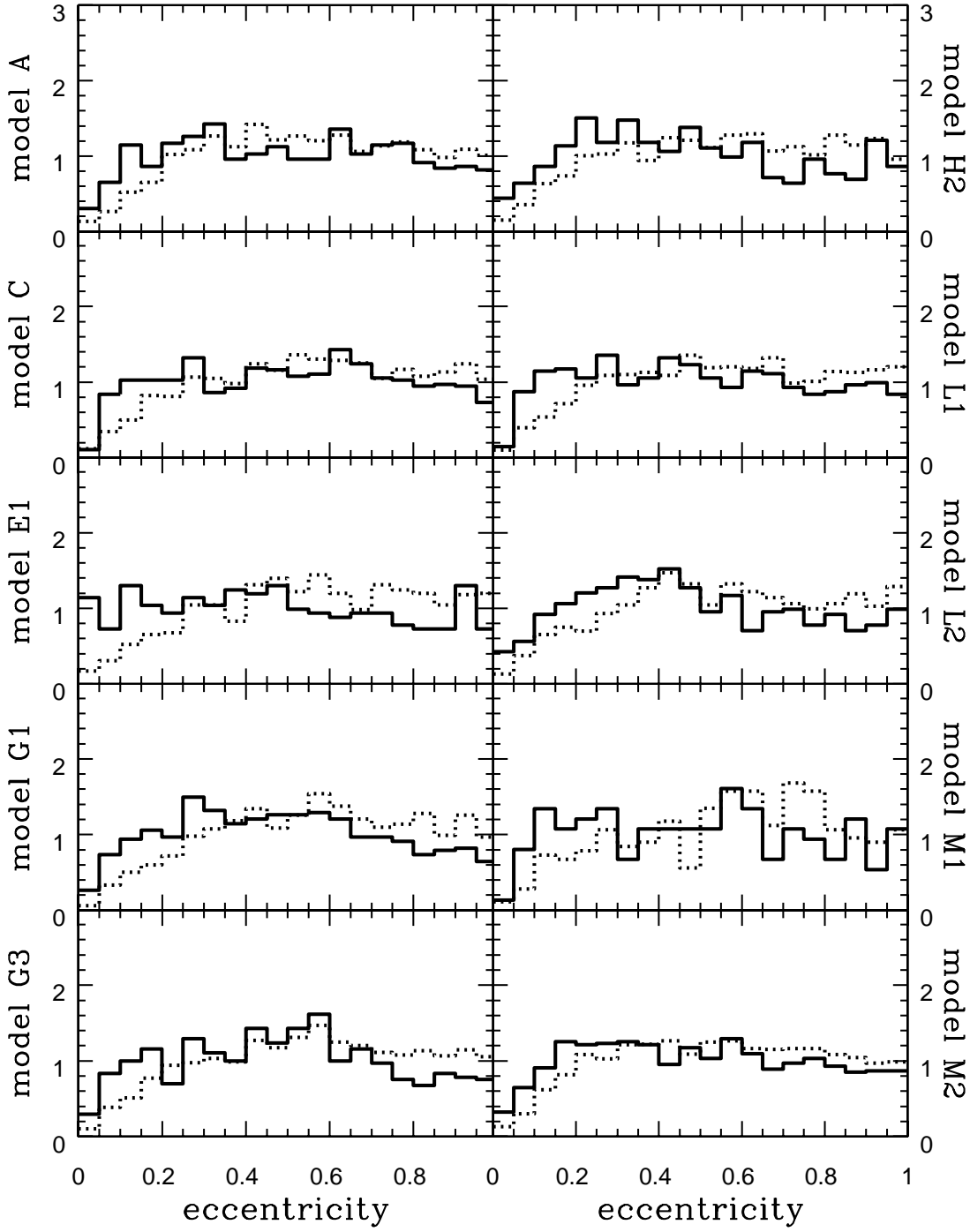


FIG. 4.— Eccentricity distribution functions for noncoalescing binaries. Line types as in Fig. 3.

model. In Bayes' law of conditional probabilities:

$$P(M|D, I) = \frac{P(D|M, I)}{P(D, I)} P(M, I), \quad (2)$$

where  $P(M|D, I)$  is the *posterior* probability, i.e., the probability associated with a model  $M$ , given the data

set  $D$ ;  $P(D|M, I)$  is the *likelihood* of the data set, given a model and we will denote by  $\Lambda(D)$ .  $P(M, I)$  is the *prior* probability of the model, and  $P(D|I)$  a *normalizing factor* for  $P(M|D, I)$ . This normalizing factor  $P(D|I)$  is a constant so that  $\int_M P(M|D, I) dM = 1$ , and it is

unknown at this point in the analysis.

Concerning the theoretical models consider here, we have no specific prior bias against one or another. In other words, all models  $M$  are considered equally likely a priori (in the absence of data), so  $P(M, I)$  must simply be a constant. Since this prior probability is a constant, it can be absorbed into the unknown normalizing factor  $P(D|I)$ , so that

$$P(M|D, I) = C \cdot \Lambda(D), \quad (3)$$

where  $C = P(M, I)/P(D|I)$ ,  $C$  makes  $P(M|D, I)$  a properly normalized probability density, and  $D$  in our case is the set of observed eccentricities, which we will denote as  $e_s$ .

Since the observations and property measurements for each DNS in the sample are independent, the likelihood of the complete set of measured eccentricities is equal to the product of the individual measurement likelihoods:

$$\Lambda(e_s) = \prod_i P(e_i|M, I). \quad (4)$$

$P(e_i|M, I)$  can be expressed as a convolution integral of  $P(e_i|\hat{e}, I)$  over all possible  $\hat{e}$  values, given a model  $M$ :

$$P(e_i|M, I) = \int_{\hat{e}=0}^{\hat{e}=1} P(e_i|\hat{e}, I) \times P(\hat{e}|M, I) d\hat{e}. \quad (5)$$

$P(e_i|\hat{e}, I)$  is just the Gaussian expression given in § 4.1.1 for the distribution of measured values given a “true” value, and  $P(\hat{e}|M, I)$  is the distribution of “true” eccentricities, which we have generated from the Monte Carlo simulations of DNS binaries for each model. Consequently, for each model, we have at hand all the ingredients we need to calculate the likelihood of the data set  $\Lambda(e_s)$ , using eqs. (4) and (5). The relevant integral is calculated numerically using our model distributions. Since  $\Lambda(e_s)$  is strictly proportional to the posterior probability of the model  $P(M|D, I)$  (see eq. [3]), we do not have to calculate the constant  $C$ , and instead we can evaluate the various models based on their likelihood values  $\Lambda(e_s)$ . The results of this evaluation is described next.

#### 4.2. Statistical Results

The full set of calculated likelihood values for various models are shown in Table 3. We note that  $\Lambda$  values are *not* normalized, so their absolute values have little meaning. However it is their comparative values that allow us to address the questions of interest to us: given the observed sample of measured DNS eccentricities, (i) are the birth or present populations more likely? (ii) which of the ten binary evolution models considered here more likely? (iii) are “standard” kick magnitudes or small or zero kicks more likely? To address each of these questions we examine the likelihood (or *odds*) ratios for the models relevant in each case and compare these ratios to unity.

##### 4.2.1. Birth vs. Present Distributions

To quantitatively compare our results for the present and birth distributions we present the model odds ratios  $\Lambda_{\text{present}}/\Lambda_{\text{birth}}$  as a function of the binary evolution models (Fig. 5). It is evident that for the majority of the models, the ratios exceed unity often by factors of more

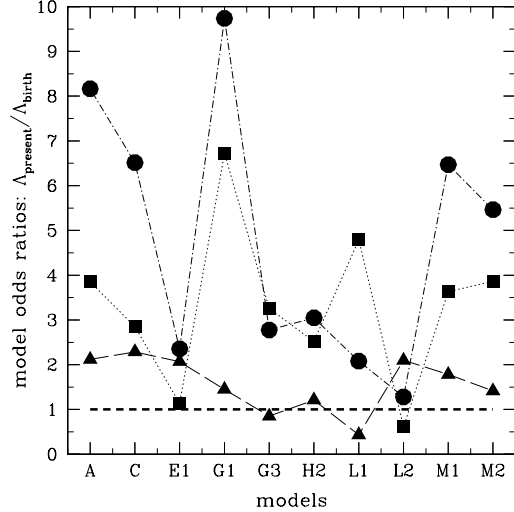


FIG. 5.— Model odds ratios for the present vs. birth distributions for each of the ten binary evolution models. The squares correspond to coalescing DNS, the triangles to noncoalescing DNS, and the circles to all systems combined.

than 2 or as high as 10. We note that for noncoalescing DNS the ratio values “hover” within a factor of 2 from unity indicating that there is little or insignificant evolution from birth to present for these wide DNS binaries (as already noted in § 3.2).

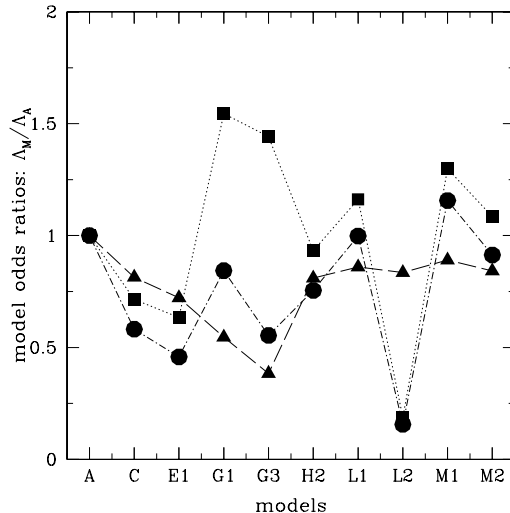
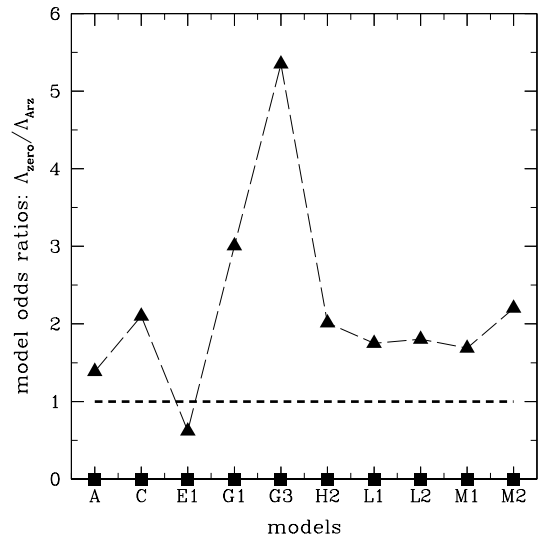
We conclude that the models for coalescing DNS provide clear evidence that orbital evolution due to gravitational radiation is important. When allowed to evolve, the roughly uniform eccentricity distribution at birth shifts to favor lower eccentricities at present. Three of the four coalescing DNS inhabit the lower eccentricity part of the distributions, so the shift towards lower eccentricities usually raises the likelihood of present model distributions over those at DNS birth. This is in full agreement with the conclusions reached by (Chaurasia & Bailes 2005) based on a different analysis and arguments. On the other hand the lack of strong bias in favor of the present distributions from the non-coalescing DNS models is understood, given their long orbital evolution timescales.

Two exceptions to high odds ratios in the coalescing systems appear for models E1 and L2 (these, respectively, assume very low common-envelope efficiency and large specific angular momentum carried by mass lost from the binary in non-conservative mass transfer phases). For model E1 (see Fig. 3), the eccentricity distribution already favors low  $e$  at birth, such that when allowed to evolve, much of the DNS population possesses  $e < 0.05$ , a region where there are no observed DNS. We also see that the probability of seeing DNS at  $0.2 < e < 0.3$  actually decreases, contributing by lowering the “present” likelihood. In model L2, the odds ratio close to unity is an indication of little evolution with time (see Fig. 3) for the DNS formed under L2 assumptions combined with a negligible change in the PDF in the range  $0.2 < e < 0.3$ .

##### 4.2.2. Preferred Binary Evolution Models

TABLE 3  
LIKELIHOOD VALUES

Model	Coalescing					Noncoalescing				
	$\Lambda_{birth}^a \times 10^{34}$	$\Lambda_{Arz}^b \times 10^{34}$	$\Lambda_{zero}^c \times 10^{34}$	$\Lambda_{10}^d \times 10^{34}$	$\Lambda_{50}^e \times 10^{34}$	$\Lambda_{birth}^a \times 10^{22}$	$\Lambda_{Arz}^b \times 10^{22}$	$\Lambda_{zero}^c \times 10^{22}$	$\Lambda_{10}^d \times 10^{22}$	$\Lambda_{50}^e \times 10^{22}$
A	0.61	2.35	0.00	0.00	0.41	1.34	2.84	3.94	6.40	3.20
C	0.59	1.68	0.00	0.00	2.33	1.01	2.31	4.85	7.05	2.99
E1	1.31	1.49	0.00	0.00	0.00	0.99	2.05	1.27	3.47	9.17
G1	0.54	3.63	0.00	0.00	2.10	1.07	1.55	4.66	4.97	2.46
G3	1.04	3.39	0.00	0.00	3.09	1.28	1.09	5.83	6.42	2.96
H2	0.87	2.19	0.00	0.00	0.00	1.90	2.30	4.63	6.10	2.43
L1	0.57	2.73	0.00	0.00	1.22	5.62	2.44	4.27	5.65	3.76
L2	0.72	0.44	0.00	0.00	0.00	1.13	2.37	4.27	7.65	2.45
M1	0.84	3.05	0.00	0.00	0.00	1.42	2.53	4.27	10.68	3.81
M2	0.66	2.55	0.00	0.00	1.49	1.69	2.39	5.26	6.71	3.43

<sup>a</sup> $\Lambda$  values at birth for Arzoumanian kick distribution.<sup>b</sup> $\Lambda$  values at present for Arzoumanian kicks.<sup>c</sup> $\Lambda$  values at present for zero NS kicks.<sup>d</sup> $\Lambda$  values at present for a  $\sigma = 10 \text{ km s}^{-1}$  Maxwellian kick distribution.<sup>e</sup> $\Lambda$  values at present for a  $\sigma = 50 \text{ km s}^{-1}$  Maxwellian kick distribution.FIG. 6.— Model odds ratios for present distributions and for all models normalized to the standard model A:  $\Lambda_{present,M}$  values for all models, normalized to  $\Lambda_{present,A}$ . Again, the squares mark coalescing binaries, the triangles noncoalescing, and dots combine both coalescing and noncoalescing binaries.FIG. 7.— Model odds ratios,  $\Lambda_{zero}/\Lambda_{Arz}$  for all models. The squares mark the coalescing binaries; the triangles correspond to noncoalescing systems

Guided by our conclusion that the present distributions are more likely, given the measurements, we compare the present likelihoods of the various binary evolution models to that of the standard model A (see Fig. 6). It is interesting to note that for the majority of the models the ratios are well within a factor of 2 from unity. There is only one exception and this is model L2 with the assumed high specific angular momentum of mass lost in non-conservative mass transfer: its odds ratios for the coalescing population compared to model A is lower than 0.25. We conclude that the sample of measured DNS eccentricities is not a strong tool for distinguishing between binary evolution models; the great majority of the ones considered here appear quantitatively consistent with the eccentricity measurements, with the sole exception of L2.

#### 4.2.3. Zero and Low Kick Distributions

Last we examine whether the origin of the low eccentricities is related to unexpectedly low or zero kicks imparted to NS at birth. In Table 3 we list the likelihood values for all ten models and for models with zero or low kick-magnitude distributions at present. In Fig. 7 the model odds ratios for the zero kicks vs. Arzoumanian kicks, as an example of an illustration.

In the case of noncoalescing DNS the ratios for most of the models are within or very close to a factor of 2 from unity, with the exception of two models (G1 and G3). This could tentatively be used as an argument in favor of the hypothesis of very small NS kicks. However, it is most interesting to examine the case of coalescing binaries: the likelihood values are *exactly equal to zero*, for all ten models with either zero kicks or kicks drawn

from a  $\sigma = 10 \text{ km s}^{-1}$  Maxwellian, and for four models with kicks drawn from a  $\sigma = 50 \text{ km s}^{-1}$  Maxwellian. As a result all these models are rendered *very highly unlikely*. The reason for these values being identically zero can be traced back to the properties of the Hulse-Taylor binary PSR B1913+16: it has an eccentricity of 0.617 and all the models above have distributions such that the probability for  $e \gtrsim 0.5$  is identically zero (see Fig. 1). Therefore, these models cannot allow for the existence of PSR B1913+16, and consequently their likelihood becomes equal to zero.

Based on the results for coalescing DNS, we conclude that models with vanishingly or moderately small kicks ( $\sigma \lesssim 50 \text{ km s}^{-1}$ ) are inconsistent with the current observed sample.

## 5. CONCLUSIONS AND DISCUSSION

We addressed the question of the origin of the low eccentricities measured for observed DNS binaries (close and wide) that has attracted considerable attention in the recent literature (van den Heuvel 2004; Chaurasia & Bailes 2005). We use DNS population models and associated predictions for eccentricity distributions along with a Bayesian statistical analysis and quantitative comparison with the observed sample. We conclude that for the case of close (coalescing) DNS binaries, models with vanishingly or moderately small kicks ( $\sigma \lesssim 50 \text{ km s}^{-1}$ ) can be excluded as inconsistent with the current observed sample (and specifically the Hulse-Taylor binary pulsar). We also examine the influence of orbital evolution due to gravitational radiation from the time of DNS birth to the present. We conclude that model distributions of DNS eccentricities *at present* are significantly more likely, given the observed sample. Our conclusion holds for the great majority of the models examined, unless the birth properties are such that there is very little orbital evolution from birth to the present. These results are in agreement with the conclusions obtained by Chaurasia & Bailes (2005) previously based on different methods of analysis.

As also noted by Chaurasia & Bailes (2005), some fraction of the systems that have high eccentricities at birth

actually end up merging very soon after (the rest of the high-eccentricity systems, evolve to lower eccentricities without necessarily merging completely by the present). As seen it is evident in Fig. 10, high eccentricity systems at birth ( $0.8 < e < 1.0$ ) tend to favor shorter merger times, more so than lower-e DNS. Highly eccentric DNS have accelerated orbital decay due to strong gravitational wave emission at periastron and due to their early mergers are not likely to be represented in the observed sample (as is the case for our Galaxy). The importance of such short-lived systems has also been pointed in the past.

Current estimates of Galactic DNS merger rates (of interest to ground-based gravitational-wave interferometers like LIGO) are based on the DNS observed sample and do not account for this selection effect against high-eccentricity DNS with short merger times (see Kalogera et al. (2004) and references therein). Consequently these rate estimates could underestimate the true merger rate by possibly a significant factor. This issue has in fact pointed out in the past in a somewhat different context (see Belczynski & Kalogera (2001) and Ivanova et al. (2003)). To assess the magnitude of this upward correction factor that should in principle be applied to such rate estimates, we calculate the fraction of DNS with merger times (at birth) shorter than 1 Myr and 10 Myr. We find that in most models these fractions are  $\simeq 10 - 15\%$  and  $\simeq 20 - 30\%$ , respectively; for a couple of our extreme models (C and E1) the fractions are  $\simeq 50\%$  for a cut of 10 Myr. We conclude that although orbital evolution due to gravitational radiation affects the eccentricity distribution of the observed sample, the associated upwards correction factor to merger rate estimates is rather small (typically 10-40%). This factor is well within the current uncertainties of the DNS merger rate estimates for the Galaxy.

We thank Bart Willems for useful discussions. This work has been supported by NSF Gravitational Physics grant PHYS-0353111 and a David and Lucile Packard Foundation Fellowship in Science and Engineering to VK.

## REFERENCES

Arzoumanian, Z., Chernoff, D. F., Cordes, J. M. 2001, ApJ  
 Belczynski, K., Kalogera, V. 2001, ApJ, 550, L183  
 Belczynski, K., Kalogera, V., Bulik, T. 2001, ApJ, 572, 407  
 Belczynski, K., et al. 2005, ApJ, to be submitted  
 Burgay, M., D'Amico, N., Possenti, A., Manchester, R. N., Lyne, A. G., Joshi, B. C., McLaughlin, M. A., Kramer, M., Sarkissian, J. M., Camilo, F., Kalogera, V., Kim, C. and Lorimer, D. R. 2003, Nature, 426, 531  
 Champion, D. J., Lorimer, D. R., McLaughlin, M. A., Cordes, J. M., Arzoumanian, Z., Weisberg, J. M., Taylor, J. H. 2004, MNRAS, 350, 61  
 Chaurasia, H. K., Bailes, M. 2005, ApJ, in press  
 Faulkner, A. J., Kramer, M., Lyne, A. G., Manchester, R. N., McLaughlin, M. A., Stairs, I. H., Hobbs, G., Possenti, A., Lorimer, D. R., D'Amico, N., Camilo, F., and Burgay, M. 2004, ApJ, 618, 119  
 Finn, L. S. 1994, Phys. Rev. Lett., 73, 1878  
 Hobbs, G., Lorimer, D. R., Lyne, A. G., Kramer, M. 2005, MNRAS, 360, 963  
 Hulse, R. A., Taylor, J. H. 1975, ApJ, 195, L51  
 Ivanova, N., Belczynski, K., Kalogera, V., Rasio, F., Taam, R.E. 2003, ApJ, 592, 475  
 Kalogera, V. 1996, ApJ, 471, 352  
 Kalogera, V., Kim, C., Lorimer, D. R., Burgay, M., D'Amico, N., Possenti, A., Manchester, R. N., Lyne, A. G., Joshi, B. C., McLaughlin, M. A., Kramer, M., Sarkissian, J. M., Camilo, F. 2004, ApJ, 614, L137  
 Lyne, A. G., Camilo, F., Manchester, R. N., Bell, J. F., Kaspi, V. M., D'Amico, N., McKay, N. P. F., Crawford, F., Morris, D. J., Sheppard, D. C., Stairs, I. H., 2000, MNRAS, 312, 4, 698  
 Lyne, A. G., Lorimer, D. R. 1994, Nature, 369, 127  
 Nice, D. J., Sayer, R. W., Taylor, J. H. 1996, ApJ  
 Peters, P.C. 1964, Physical Review, 136, 1224  
 Pfahl, E., Rappaport, S., Podsiadlowski, P., Spruit, H. 2002, ApJ, 574, 364  
 Phinney, E. S., Sigurdsson, S. 1991, Nature, 349, 220  
 Stairs, I. H., Manchester, R. N., Lyne, A. G., Kaspi, V. M., Camilo, F., Bell, J. F., D'Amico, N., Kramer, M., Crawford, F., Morris, D. J., Possenti, A., McKay, N. P. F., Lumsden, S. L., Tacconi-Garman, L. E., Cannon, R. D., Hambly, N. C., Wood, P.R. 2001, MNRAS, 325, 979  
 Timmes, F. X., Woosley, S. E., Weaver, T. A. 1996, ApJ, 457, 834  
 van den Heuvel, E. P. J. 2004, to appear in proceedings Fifth Integral Science Workshop  
 Wolszczan, A. 1991, Nature, 350, 688

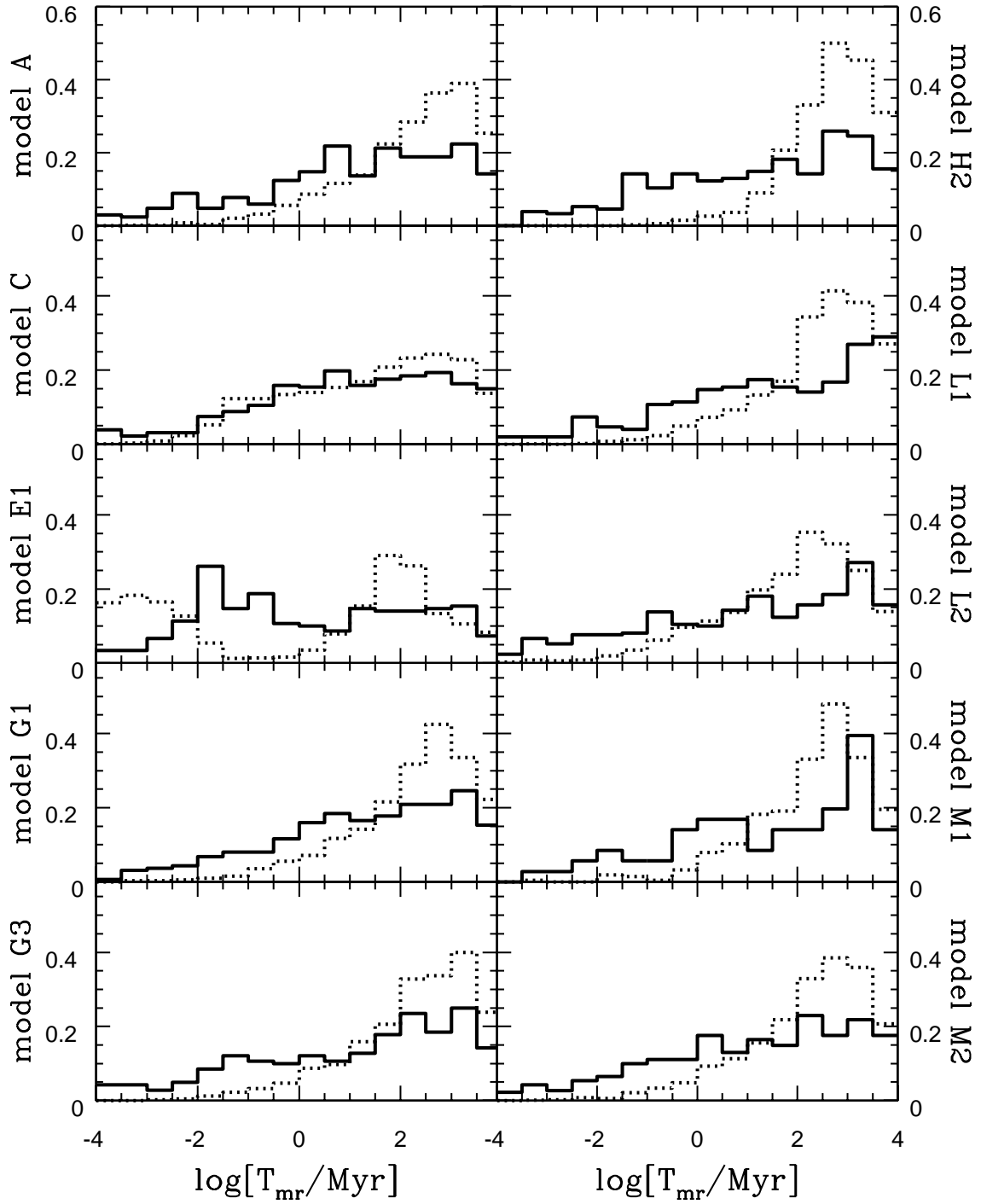


FIG. 8.— The birth distributions of  $T_{mr}$  for each model and for two eccentricity ranges: 0-0.8 (dotted lines) and 0.8-1.0 (solid lines). Arzoumanian kicks assumed.